

# Whistler-mode waves excited by anisotropic hot electrons with a drift velocity in Earth's magnetosphere: Linear theory

Jun guo<sup>1</sup>, Kai Fan<sup>2</sup>, and Jicheng Sun<sup>3</sup>

<sup>1</sup>Qingdao University of Science and Technology

<sup>2</sup>University of Science and Technology of China

<sup>3</sup>Auburn University

November 24, 2022

## Abstract

With a linear theoretical model, we have investigated the properties of whistler waves excited by anisotropic hot electrons with a drift velocity, which is usually neglected in previous studies. It is found that a finite drift velocity can significantly change the properties of excited whistler waves, resulting in distinct properties for parallel and antiparallel propagating waves. In the high-beta regime, as the drift velocity increases, the frequency of parallel propagating whistler waves increases, while that of antiparallel propagating waves is found to decline. So parallel and antiparallel propagating whistler waves appear in different frequency bands. However, the growth rate of parallel wave is always smaller than that of antiparallel wave, and falls below  $10\Omega$  for large drift velocities ( $v/v > 1.5$ ), in which case the parallel wave may be too weak to be observed. Generally, the growth rate of whistler waves in both directions is enhanced with the increasing anisotropy or proportion of hot electrons. In the low-beta regime, the trends of the frequency and linear growth rate of excited whistler waves are quite similar to those in the high-beta regime. But, with the increase of the drift velocity, the wave normal angle of parallel propagating whistler waves gradually declines until reaching zero, while that of antiparallel propagating waves continues to increase. Our study may help people to better understand various whistler-mode spectra observed in the Earth's magnetosphere.

1           **Whistler-mode waves excited by anisotropic hot**  
2                   **electrons with a drift velocity in Earth's**  
3                           **magnetosphere: Linear theory**

4                                   Kai Fan<sup>1,2</sup>, Jicheng Sun<sup>3</sup>, and Jun Guo<sup>4\*</sup>

5           <sup>1</sup>CAS Key Laboratory of Geospace Environment, Department of Geophysics and  
6           Planetary Science, University of Science and Technology of China, Hefei 230026,  
7           China

8           <sup>2</sup>Shandong Provincial Key Laboratory of Optical Astronomy and Solar-Terrestrial  
9           Environment, Shandong University, Weihai, 264209, China

10          <sup>3</sup>Physics Department, Auburn University, Auburn, Alabama, USA

11          <sup>4</sup> College of Mathematics and Physics, Qingdao University of Science and  
12          Technology, Qingdao, 266061, China

13          \*Email: guoj2005@163.com

## Abstract

14

15       With a linear theoretical model, we have investigated the properties of whistler  
16 waves excited by anisotropic hot electrons with a drift velocity, which is usually  
17 neglected in previous studies. It is found that a finite drift velocity can significantly  
18 change the properties of excited whistler waves, resulting in distinct properties for  
19 parallel and antiparallel propagating waves. In the high-beta regime, as the drift  
20 velocity increases, the frequency of parallel propagating whistler waves increases,  
21 while that of antiparallel propagating waves is found to decline. So parallel and  
22 antiparallel propagating whistler waves appear in different frequency bands.  
23 However, the growth rate of parallel wave is always smaller than that of antiparallel  
24 wave, and falls below  $10^{-2}\Omega_e$  for large drift velocities ( $v_d/v_{th} > 1.5$ ), in which  
25 case the parallel wave may be too weak to be observed. Generally, the growth rate of  
26 whistler waves in both directions is enhanced with the increasing anisotropy or  
27 proportion of hot electrons. In the low-beta regime, the trends of the frequency and  
28 linear growth rate of excited whistler waves are quite similar to those in the  
29 high-beta regime. But, with the increase of the drift velocity, the wave normal angle  
30 of parallel propagating whistler waves gradually declines until reaching zero, while  
31 that of antiparallel propagating waves continues to increase. Our study may help  
32 people to better understand various whistler-mode spectra observed in the Earth's  
33 magnetosphere.

## 34 1. Introduction

35 Whistler-mode waves, also known as chorus waves, are one of the most intense  
36 natural emissions at frequencies between  $0.1$  and  $0.8f_{ce}$  ( $f_{ce}$  is the equatorial electron  
37 gyrofrequency) in the Earth's magnetosphere (Burtis and Helliwell, 1969; Tsurutain &  
38 Smith, 1974; Li et al., 2012). They have received much attention due to their key role  
39 in controlling electron dynamics in the Earth's Van Allen radiation belt. Chorus waves  
40 have been commonly believed to account for both the precipitation of low-energy  
41 ( $0.1$ - $30$ keV) electrons into atmosphere (Thorne et al., 2010; Ni et al., 2011; Nishimura  
42 et al., 2013) and the dominant source of relativistic electrons ( $\sim$ MeV) in the heart of  
43 radiation belt during geoactive periods (Summers et al., 2002; Reeves et al., 2013;  
44 Thorne et al., 2013). In the spectrogram, whistler-mode chorus waves are typically  
45 divided into two separated bands by a power gap around  $0.5f_{ce}$  (Meredith et al., 2001;  
46 Ratcliffe and Watt, 2017): lower band ( $0.1f_{ce}$ - $0.5f_{ce}$ ) and upper band ( $0.5f_{ce}$ - $0.8f_{ce}$ ).  
47 Much effort has been made to understand the formation of the power gap around  
48  $0.5f_{ce}$  (Omura et al., 2009; Fu et al., 2015; Gao et al., 2016a, 2017, 2018, 2019), but  
49 there is still no consensus reached on this issue. The majority of whistler-mode chorus  
50 waves in Earth's magnetosphere are quasi-parallel with wave normal angle (WNA)  
51 smaller than  $30^\circ$  (Li et al., 2011), while there is also a significant population of very  
52 oblique waves with WNA near the resonant angle (Li et al., 2011; Gao et al., 2016b).  
53 The main source region of whistler-mode waves is located at the magnetic equator  
54 and just extends to several degrees of magnetic latitude (Lauben et al., 2002; Santolik  
55 et al., 2005).

56 It is widely accepted that whistler-mode waves in the Earth's magnetosphere  
57 extract free energy from energetic electrons injected from plasma sheet during  
58 geoactive periods (Li et al., 2010; Gao et al., 2014). These tens of keV electrons  
59 usually have significant temperature anisotropies with  $T_{\perp} > T_{\parallel}$ , which are unstable to  
60 the whistler anisotropy instability (Lu et al., 2004, 2010; Santolik et al., 2010; Liu et  
61 al., 2011; Omura and Nunn, 2011; Gary et al., 2011; Ke et al., 2017). Hereafter, the  
62 subscripts  $\perp$  and  $\parallel$  denote the directions perpendicular and parallel to the  
63 background magnetic field. In previous studies, this energy source is often modeled as  
64 a single bi-Maxwellian distribution in velocity space without the bulk velocity. In this  
65 scenario, whistler-mode waves with parallel and anti-parallel propagating directions  
66 are simultaneously excited in the source region and have the same amplitude, which  
67 has been supported by both the linear theory and PIC simulations (Gary et al., 2011;  
68 An et al., 2017; Chen et al., 2018; Fan et al., 2019). As a result, the presence of mixed  
69 Poynting flux directions of whistler-mode chorus waves becomes a common method  
70 to determine their source region from satellite observations (LeDocq et al., 1998;  
71 Santolik et al., 2003). Besides, the wave normal angle of excited whistler-mode waves  
72 is mainly controlled by the parallel plasma beta ( $\beta_{\parallel}$ ) of anisotropic energetic electrons  
73 (Gary et al., 2011; Yue et al., 2016; An et al., 2017; Fan et al., 2019). Generally, in the  
74 high-beta ( $\beta_{\parallel} \geq 0.025$ ) regime, the WNA of whistler mode with the largest linear  
75 growth rate is always zero. While, in the low-beta ( $\beta_{\parallel} \leq 0.025$ ) regime, the WNA of  
76 the most unstable whistler mode will become very large ( $> \sim 40^{\circ}$ ).

77 Recent observations from THEMIS satellite have revealed that both

78 quasi-parallel and oblique whistler-mode chorus waves are usually detected along  
79 with a beam-like electron population in the Earth's magnetosphere (Chen et al., 2019).  
80 This implies that the bi-Maxwellian electron distribution with a drift velocity along  
81 the background magnetic field is a better model describing anisotropic energetic  
82 electrons. With a theoretical model, Mourenas et al. (2015) proposed that very oblique  
83 ( $\text{WNA} \approx \arccos^{-1} f/f_{ce}$ ) lower-band whistler waves can be generated by anisotropic  
84 electron beam through a combination of cyclotron resonance and Landau resonance.  
85 This potential mechanism has been supported by a statistical study on very oblique  
86 chorus waves (Gao et al., 2016b). However, the effect of a finite drift velocity of  
87 anisotropic energetic electrons on excited whistler waves is still not fully understood.

88 In this paper, we have comprehensively studied the properties of whistler waves  
89 excited by anisotropic electrons with a finite drift velocity along the background  
90 magnetic field with a linear theoretic model. Especially, we focus on the effects of the  
91 drift velocity on the linear growth rate, wave frequency, and WNA of excited whistler  
92 waves in both high-beta and low-beta regimes. It is found that a modest drift velocity  
93 can significantly change the properties of excited whistler waves, but the changes are  
94 quite different in two propagating directions, i.e., parallel and anti-parallel to the  
95 background magnetic field.

96 The rest of this paper is structured as follows. Section 2 describes the linear  
97 theoretical model used in this study, and theoretical results for both high-beta and  
98 low-beta regimes are presented in Section 3. Section 4 is a summary of principal

99 results.

## 100 2. Linear theoretical model

101 We have investigated the effects of the drift velocity on whistler-mode waves  
102 excited by anisotropic hot electrons using the linear theory. The WHAMP (Waves in  
103 Homogeneous Anisotropic Magnetized Plasma) model (Ronmark, 1982), which can  
104 be easily accessed on <https://github.com/irfu/whamp>, is utilized to calculate the  
105 dispersion relation of whistler mode and associated linear growth rates. This code has  
106 been widely used in previous works (Xiao et al., 2007; Chen et al., 2018; Denton,  
107 2018; Fan et al., 2019).

108 In this study, the background magnetic field  $B_0$  and plasma density  $n_{total}$  are  
109 assumed as 80 nT and  $1.0 \text{ cm}^{-3}$ , meaning the ratio between plasma frequency and  
110 gyrofrequency ( $\omega_{pe}/\Omega_e$ ) is about 4, which is a typical value in the source region of  
111 whistler-mode waves (Gao et al., 2014). In this model, there are three species in the  
112 plasma, such as cool protons, cool electrons, and hot electrons, which are denoted by  
113 subscripts “p”, “c”, and “h”, respectively. The background cool protons and cool  
114 electrons both satisfy the Maxwellian velocity distribution and have the same  
115 temperature of 1 eV. The hot electrons are the source of free energy to excite whistler  
116 waves, which are described as a drifting bi-Maxwellian distribution:

$$117 \quad f_h(v_{\perp}, v_{\parallel}) = \frac{n_h}{(2\pi)^{3/2} v_{th}^3} \exp\left[-\frac{(v_{\parallel}-v_{dh})^2}{2v_{th}^2}\right] \frac{T_{\parallel h}}{T_{\perp h}} \exp\left[-\frac{v_{\perp}^2}{2(T_{\perp h}/T_{\parallel h})v_{th}^2}\right],$$

118 where  $n$ ,  $v$ , and  $T$  represent the density, velocity, and temperature, respectively. The

119  $v_{th}$  and  $v_d$  denote the parallel thermal velocity and drift velocity of hot electrons,  
 120 respectively. Besides, the background magnetic field is along  $z$  axis, and the densities  
 121 of three species satisfy  $n_h + n_c = n_p = n_{total}$ . Note that, to perform one linear  
 122 theory calculation, we need to initialize some parameters in the WHAMP model, such  
 123 as the density, parallel beta, anisotropy, and drift velocity of each component, and  
 124  $\omega_{pe}/\Omega_e$ .

### 125 **3. Results**

126 The parallel plasma beta  $\beta_{||h}$  ( $= 2\mu_0 n_{total} k_B T_{||h} / B_0^2$ ) of hot electrons is a key  
 127 parameter controlling the WNA of excited whistler-mode waves. Previous studies  
 128 revealed that the whistler wave with the maximum growth rate undergoes a transition  
 129 from parallel to oblique propagation at a critical value ( $\sim 0.025$ ) of  $\beta_{||h}$  (Gary et al.,  
 130 2011; Yue et al., 2016; An et al., 2017; Fan et al., 2019). Therefore, we have  
 131 investigated the effects of drift velocity of hot electrons on excited whistler waves in  
 132 these two regimes with the WHAMP model.

#### 133 **3.1 High-beta Regime: $\beta_{||h} > 0.025$**

134 Since the linear growth rate of unstable whistler waves always peaks at the WNA  
 135 of  $0^\circ$  in our considered cases, we only consider parallel and antiparallel propagating  
 136 whistler waves in this regime. Figure 1 exhibits the frequency  $\omega/\Omega_e$  (black lines)  
 137 and linear growth rate  $\gamma/\Omega_e$  (red lines) of whistler waves as a function of parallel  
 138 wave number  $k_{||} v_{th} / \Omega_e$  for two cases with different relative drift velocities: (a)

139  $v_d = 0$  and (b)  $v_d = 1.0v_{th}$ . In two cases, the parallel plasma beta  $\beta_{||h}$ , anisotropy  
 140  $T_{\perp h}/T_{||h}$ , number density  $n_h/n_{total}$  of hot electrons are fixed as 0.32, 4, and 0.1,  
 141 respectively. Hereafter, solid and dashed lines represent whistler waves that propagate  
 142 parallel and antiparallel to the background magnetic field, respectively. Just as  
 143 expected, without the drift velocity, the whistler waves driven by anisotropic hot  
 144 electrons have the same dispersion relation and linear growth rate in parallel and  
 145 antiparallel directions (Figure 1a). In Figure 1a, the frequency  $\omega/\Omega_e$  and linear  
 146 growth rate  $\gamma/\Omega_e$  of the most unstable whistler wave are 0.46 and 0.035 in both  
 147 directions. However, when anisotropic electrons are given a drift velocity of  $1.0v_{th}$   
 148 in Figure 1b, the properties of unstable whistler waves have changed significantly. For  
 149 parallel propagating waves, the most unstable whistler mode now has a higher  
 150 frequency of  $0.61\Omega_e$  ( $>0.5\Omega_e$ ) but a smaller linear growth rate of  $0.019\Omega_e$ . While, for  
 151 antiparallel propagating waves, the most unstable whistler mode has a lower  
 152 frequency of  $0.3\Omega_e$  ( $<0.5\Omega_e$ ) but a larger linear growth rate of  $0.036\Omega_e$ . As a result,  
 153 there exist obvious differences between parallel and antiparallel propagating waves,  
 154 making it very easy to distinguish them in the spectrogram. That is, parallel  
 155 propagating whistler waves fall within upper band ( $>0.5\Omega_e$ ) and have smaller  
 156 amplitudes, but antiparallel propagating waves belong to lower band ( $<0.5\Omega_e$ ) and  
 157 have larger amplitudes.

158 The pitch-angle distribution of electrons for two cases are shown in Figure 2.  
 159 The coded color denotes the velocity of electrons. As shown in Figure 2a, without the  
 160 drift velocity of hot electrons, the phase space density (PSD) of electrons at a fixed

161 velocity exhibits a symmetric distribution about the pitch angle of  $90^\circ$ , and just peaks  
162 at  $90^\circ$  due to the temperature anisotropy. In Figure 2b, there is a drift velocity of  
163  $1.0v_{th}$  along the background magnetic field, so the pitch-angle distribution entirely  
164 move toward smaller pitch angles, making the profile of PSD becomes asymmetric.  
165 The maximum PSD is not at the pitch angle of  $90^\circ$  but shifts toward smaller pitch  
166 angles. And the peak of PSD of lower-energy electrons is farther away from  $90^\circ$   
167 pitch angle. Therefore, the asymmetric pitch-angle distribution can be considered as  
168 an identity of drifting anisotropic electrons in observation data.

169 Figure 3 gives a summary plot, including the effects of drift velocity  $v_d/v_{th}$ ,  
170 anisotropy  $T_{\perp h}/T_{\parallel h}$ , proportion  $n_h/n_{total}$  of hot electrons on the frequency  $\omega_d/\Omega_e$   
171 (left column) and growth rate  $\gamma_d/\Omega_e$  of most unstable whistler mode in both parallel  
172 (solid lines) and antiparallel (dashed lines) directions, respectively. Except the  
173 parameter of interest, such as  $v_d/v_{th}$ ,  $T_{\perp h}/T_{\parallel h}$ , and  $n_h/n_{total}$ , other initial  
174 parameters are fixed as those in the case shown in Figure 1b. With the increase of drift  
175 velocity, as shown in Figure 1a, the frequency of parallel propagating whistler  
176 continuously increases, while that of antiparallel propagating whistler is found to  
177 decline. As a result, the parallel and antiparallel propagating whistler will be observed  
178 in upper and lower band in the spectrogram, respectively. And a power gap between  
179 them is naturally formed. However, the growth rate of parallel whistler is always  
180 smaller than that of antiparallel wave for nonzero drift velocities, and further smaller  
181 for a larger drift velocity (Figure 3b). It is worth mentioning, since the growth rate of  
182 parallel whistler is quite small ( $\gamma_d/\Omega_e < 10^{-2}$ ) for a large drift velocity ( $v_d/v_{th} >$

183 1.5), then the parallel wave may be too weak to be observed in such case.

184 With a fixed drift velocity of  $1v_{th}$ , the frequency difference between parallel  
185 and antiparallel propagating whistler waves seems to be independent on the  
186 anisotropy and proportion of hot electrons (Figures 3c and 3e). Generally, the growth  
187 rate of whistler waves in both directions will increase as the  $T_{\perp h}/T_{\parallel h}$  or  $n_h/n_{total}$   
188 increases (Figures 3d and 3f). However, there are still two things should be pointed  
189 out. Firstly, when the  $T_{\perp h}/T_{\parallel h}$  is below  $\sim 2.5$ , the growth rate of parallel wave is  
190 somehow larger than that of antiparallel wave, but their growth rates become a very  
191 low level (Figure 3d). Then, if the  $n_h/n_{total}$  is reduced below  $\sim 5$ , there may be only  
192 lower-band (or antiparallel propagating) whistler waves excited in the system due to  
193 the low growth rate of parallel waves (Figure 3f).

### 194 **3.2 Low-beta Regime: $\beta_{\parallel h} < 0.025$**

195 Figure 4 displays the frequency  $\omega_m$  (black lines) and linear growth rate  $\gamma_m$   
196 (red lines) as a function of WNA  $\theta$  for two cases with different relative drift  
197 velocities: (a)  $v_d = 0$  and (b)  $v_d = 0.5v_{th}$ . Here  $\omega_m$  and  $\gamma_m$  denote the frequency  
198 and growth rate of whistler mode with the maximum linear growth rate at each WNA.  
199 In Figure 4a, similar to results in Figure 1a, parallel and antiparallel propagating  
200 whistler waves also have the same frequency and growth rate, but the linear growth  
201 rate peaks at the large WNA ( $\sim 40^\circ$ ) in this low-beta regime. If given a drift velocity  
202 of  $0.5v_{th}$  as shown in Figure 4b, the most unstable whistler wave in parallel  
203 direction will have the smaller WNA ( $\sim 28^\circ$ ) and linear growth rate ( $\sim 0.0094\Omega_e$ ) but

204 larger frequency, while that in antiparallel direction will have the larger WNA ( $\sim 47^\circ$ )  
205 and linear growth rate ( $\sim 0.0135\Omega_e$ ) but lower frequency. In the same format as  
206 Figure 2, Figure 5 gives the pitch-angle distribution of hot electrons for above two  
207 cases. One this to keep in mind is that the pitch-angle distribution of hot electrons will  
208 become asymmetric in the presence of a finite drift velocity (Figure 5b).

209 In low-beta regime, we have investigated not only the effects of drift velocity,  
210 anisotropy, proportion of hot electrons on the frequency and growth rate of most  
211 unstable whistler mode in both directions but also the WNA, which are presented in  
212 Figure 6. Except the parameter of interest, such as  $v_d/v_{th}$ ,  $T_{\perp h}/T_{\parallel h}$ , and  $n_h/n_{total}$ ,  
213 other initial parameters are fixed as those in the case shown in Figure 4b. In Figures  
214 1a-1c, for parallel propagating whistler wave (solid lines), as the drift velocity  
215 increases, the frequency increases but the growth rate and WNA decreases. But, the  
216 trend for antiparallel propagating whistler wave (dashed lines) is totally opposite. So  
217 the differences between parallel and antiparallel waves in frequency, growth rate, and  
218 WNA will become more significant with the increase of drift velocity. Specifically,  
219 with a finite drift velocity, the anisotropic hot electrons can simultaneously generate  
220 the quasi-parallel and very oblique whistler waves within the source region (Figure  
221 6c). The frequency and wave normal angle of excited whistler waves seem to be  
222 independent on the  $T_{\perp h}/T_{\parallel h}$  and  $n_h/n_{total}$  of hot electrons (Figures 6d, 6f, 6g, and  
223 6i). But there is a clear trend that the growth rates of both parallel and antiparallel  
224 propagating whistler waves increase with the  $T_{\perp h}/T_{\parallel h}$  or  $n_h/n_{total}$  (Figures 6e and  
225 6h). It is found that the growth rate of antiparallel wave is always larger than that of

226 parallel waves, but their ratio nearly remains constant (Figures 6e and 6h).

#### 227 4. **Conclusion and Discussion**

228 In this study, we have comprehensively investigated the properties of whistler  
229 waves excited by anisotropic hot electrons with a drift velocity with a linear  
230 theoretical model. We find that a finite drift velocity can significantly modulate the  
231 properties of excited whistler waves, but cause different effects on parallel and  
232 antiparallel propagating waves. In the high-beta regime, the WNA of most unstable  
233 whistler mode remains zero, irrespective of the drift velocity. As the drift velocity  
234 increases, the frequency of parallel propagating whistler wave increases, while that of  
235 antiparallel propagating wave is found to decline. As a result, parallel and antiparallel  
236 propagating whistler waves appear in the upper and lower bands, respectively.  
237 However, the growth rate of parallel wave is always smaller than that of antiparallel  
238 wave, and falls below  $10^{-2}\Omega_e$  for large drift velocities ( $v_d/v_{th} > 1.5$ ), in which  
239 case the parallel wave may be too weak to be observed. Generally, the growth rate of  
240 whistler waves in both directions will increase with the increasing anisotropy or  
241 proportion of hot electrons. In the low-beta regime, the trends of the frequency and  
242 linear growth rate of excited whistler waves are quite similar to those in the high-beta  
243 regime. But, with the increase of the drift velocity, the WNA of parallel propagating  
244 whistler waves gradually decline until reaching zero, while that of antiparallel  
245 propagating waves continues to increase.

246 In previous studies, the energy source that drives the excitation of whistler waves

247 in the inner magnetosphere is commonly modeled as energetic electrons satisfying  
248 the bi-Maxwellian velocity distribution (Santolik et al., 2010; Liu et al., 2011; Gary  
249 et al., 2011; Yue et al., 2016; An et al., 2017; Fan et al., 2019), and the  
250 frequency-time spectrogram is expected to be identical in parallel and antiparallel  
251 directions. However, according to our results, the parallel and antiparallel  
252 propagating whistler waves will exhibit quite different properties in the presence of  
253 the drift velocity of energetic electrons, such as the frequency, amplitude (or growth  
254 rate), and WNA. In the high-beta regime, the generated whistler waves can show up  
255 in different frequency bands (Figures 1 and 3), i.e., lower and upper bands, leaving a  
256 power gap between them. This could be another potential mechanism to explain the  
257 banded spectrum observed in magnetosphere. In the low-beta regime, both  
258 quasi-parallel and oblique whistler waves can be excited at the same time from one  
259 energy source (Figures 4 and 6). Besides, whistler waves are also frequently  
260 observed in association with magnetic reconnections at the magnetopause or  
261 magnetotail (Deng and Matsumoto, 2001; Wei et al., 2007; Huang et al., 2016; Cao  
262 et al., 2017; Wang et al., 2019), where the drift velocity of energized electrons is  
263 typically large. Therefore, our study may provide some new insights in  
264 understanding various whistler-mode spectra detected in the Earth's magnetosphere.

## 265 **Acknowledgement**

266 This work is supported by the Shandong Provincial National Natural Science  
267 Foundation (ZR2017MD012), and the Specialized Research Fund for Shandong

268 Provincial Key Laboratory. No simulation and observational data are used in this  
269 work.

## 270 **References**

271 An, X., C. Yue, J. Bortnik, V. Decyk, W. Li, and R. M. Thorne (2017), On the  
272 parameter dependence of the whistler anisotropy instability, *J. Geophys. Res.*  
273 *Space Physics*, 122, 2001–2009, doi:10.1002/2017JA023895.

274 Burtis, W. J., and R. A. Helliwell (1969), Banded chorus a new type of VLF radiation  
275 observed in the magnetosphere by OGO 1 and OGO 3. *Journal of Geophysical*  
276 *Research*, 74(11), 3002-3010. <https://doi.org/10.1029/JA074i011p03002>.

277 Cao, D., et al. (2017), MMS observations of whistler waves in electron diffusion  
278 region, *Geophys.Res.Lett.*,44, 3954-3962, doi:10.1002/2017GL072703.

279 Chen, H. Y., X. L. Gao, Q. M. Lu, J. C. Sun, and S. Wang (2018), Nonlinear  
280 evolution of counter-propagating whistler mode waves excited by anisotropic  
281 electrons within the equatorial source region: 1-D PIC simulations. *Journal of*  
282 *Geophysical Research: Space Physics*, 123, 1200 – 1207.  
283 <https://doi.org/10.1002/2017JA024850>.

284 Chen, R., X. L. Gao, Q. M. Lu, and S. Wang (2019), Unraveling the correlation  
285 between chorus wave and electron beam-like distribution in the Earth's  
286 magnetosphere. *Geophysical Research Letters*, 46, <https://doi.org/10.1029/>

287 2019GL085108.

288 Deng, X. H., and H. Matsumoto (2001), Rapid magnetic reconnection in the Earth's  
289 magnetosphere mediated by whistler waves, *Nature*, 410, 557–560,  
290 doi:10.1038/35069018.

291 Denton, R. E. (2018), Electromagnetic ion cyclotron wavefields in a realistic dipole  
292 field. *Journal of Geophysical Research: Space Physics*, 123, 1208 – 1223.  
293 <https://doi.org/10.1002/2017JA024886>.

294 Fan, K., X. L. Gao, Q. M. Lu, J. Guo, and S. Wang (2019), The effects of thermal  
295 electrons on whistler mode waves excited by anisotropic hot electrons: Linear  
296 theory and 2-D PIC simulations. *Journal of Geophysical Research: Space*  
297 *Physics*, 124. <https://doi.org/10.1029/2019JA026463>.

298 Fu, X., Z. Guo, C. Dong, and S. P. Gary (2015), Nonlinear subcyclotron resonance as  
299 a formation mechanism for gaps in banded chorus, *Geophys. Res. Lett.*, 42,  
300 3150-3159, doi:10.1002/2015GL064182.

301 Gao, X. L., W. Li, R. M. Thorne, J. Bortnik, V. Angelopoulos, Q. M. Lu, X. Tao, and  
302 S. Wang (2014), New evidence for generation mechanisms of discrete and  
303 hiss-like whistler mode waves. *Geophysical Research Letters*, 41, 4805 – 4811.  
304 <https://doi.org/10.1002/2014GL060707>.

305 Gao, X. L., Q. M. Lu, J. Bortnik, W. Li, L. J. Chen, and S. Wang (2016a), Generation

306 of multiband chorus by lower band cascade in the Earth's magnetosphere.  
307 Geophysical Research Letters, 43, 2343–2350.  
308 <https://doi.org/10.1002/2016GL068313>.

309 Gao, X., D. Mourenas, W. Li, A. V. Artemyev, Q. M. Lu, X. Tao, and S. Wang  
310 (2016b), Observational evidence of generation mechanisms for very oblique  
311 lower band chorus using THEMIS waveform data, *J. Geophys. Res. Space*  
312 *Physics*, 121, 6732–6748.

313 Gao, X. L., Y. G. Ke, Q. M. Lu, L. J. Chen, and S. Wang (2017), Generation of  
314 multiband chorus in the Earth's magnetosphere: 1-D PIC simulation.  
315 Geophysical Research Letters, 44, 618–624.  
316 <https://doi.org/10.1002/2016GL072251>.

317 Gao, X. L., Q. M. Lu, and S. Wang (2018), Statistical results of multiband chorus by  
318 using THEMIS waveform data. *Journal of Geophysical Research: Space Physics*,  
319 123, 5506–5515. <https://doi.org/10.1029/2018JA025393>.

320 Gao, X. L., L. J. Chen, W. Li, Q. M. Lu, and S. Wang (2019), Statistical results of the  
321 power gap between lower-band and upper-band chorus waves. *Geophysical*  
322 *Research Letters*, 46, 4098–4105. <https://doi.org/10.1029/2019GL082140>.

323 Gary, S. P., K. Liu, and D. Winske (2011), Whistler anisotropy instability at low  
324 electron: Particle-in-cell simulations, *Phys. Plasmas*, 18(8), 082902,  
325 [doi:10.1063/1.3610378](https://doi.org/10.1063/1.3610378).

326 Huang, S. Y., et al. (2016), Two types of whistler waves in the hall reconnection  
327 region, *J. Geophys. Res. Space Physics*, 121, 6639–6646,  
328 doi:10.1002/2016JA022650.

329 Ke, Y. G., X. L. Gao, Q. M. Lu, X. Y. Wang, and S. Wang (2017), Generation of  
330 rising-tone chorus in a two-dimensional mirror field by using the general  
331 curvilinear PIC code. *Journal of Geophysical Research: Space Physics*, 122,  
332 8154–8165. <https://doi.org/10.1002/2017JA024178>.

333 Lauben, D. S., U. S. Inan, T. F. Bell, and D. A. Gurnett (2002), Source characteristics  
334 of ELF/VLF chorus, *J. Geophys. Res.*, 107(A12), 1429,  
335 doi:10.1029/2000JA003019.

336 LeDocq, M. J., D. A. Gurnett, and G. B. Hospodarsky (1998), Chorus source  
337 locations from VLF Poynting flux measurements with the Polar spacecraft.  
338 *Geophysical Research Letters*, 25(21), 4063–4066.  
339 <https://doi.org/10.1029/1998GL900071>.

340 Li, W., R. M. Thorne, Y. Nishimura, J. Bortnik, V. Angelopoulos, J. P. McFadden, et  
341 al. (2010). THEMIS analysis of observed equatorial electron distributions  
342 responsible for the chorus excitation. *Journal of Geophysical Research*, 115,  
343 A00F11. <https://doi.org/10.1029/2009JA014845>.

344 Li, W., J. Bortnik, R. M. Thorne, and V. Angelopoulos (2011), Global distribution of  
345 wave amplitudes and wave normal angles of chorus waves using THEMIS wave

346 observations, *J. Geophys. Res.*, 116, A12205, doi:10.1029/2011JA017035.

347 Li, W., R. M. Thorne, J. Bortnik, X. Tao, and V. Angelopoulos (2012),  
348 Characteristics of hiss-like and discrete whistler-mode emissions. *Geophysical*  
349 *Research Letters*, 39, L18106. <https://doi.org/10.1029/2012GL053206>.

350 Liu, K., S. P. Gary, and D. Winske (2011), Excitation of banded whistler waves in the  
351 magnetosphere, *Geophys. Res. Lett.*, 38, L14108, doi:10.1029/2011GL048375.

352 Lu, Q. M., L. Q. Wang, Y. Zhou, and S. Wang (2004), Electromagnetic instabilities  
353 excited by electron temperature anisotropy, *Chin. Phys. Lett.*, 21, 129-132.

354 Lu, Q. M., L. H. Zhou, and S. Wang (2010), Particle-in-cell simulations of whistler  
355 waves excited by an electron  $\kappa$  distribution in space plasma, *J. Geophys. Res.*,  
356 115, A02213, doi:10.1029/2009JA014580.

357 Meredith, N. P., R. B. Horne, and R. R. Anderson (2001), Substorm dependence of  
358 chorus amplitudes: Implications for the acceleration of electrons to relativistic  
359 energies. *Journal of Geophysical Research*, 106(A7), 13,165–13,178.  
360 <https://doi.org/10.1029/2000JA900156>.

361 Mourenas, D., A. V. Artemyev, O. V. Agapitov, V. Krasnoselskikh, and F. S. Mozer  
362 (2015), Very oblique whistler generation by low-energy electron streams, *J.*  
363 *Geophys. Res. Space Physics*, 120, 3665–3683, doi:10.1002/2015JA021135.

364 Ni, B. B., R. M. Thorne, Y. Y. Shprits, K. G. Orlova, and N. P. Meredith (2011),

365 Chorus-driven resonant scattering of diffuse auroral electrons in nondipolar  
366 magnetic fields. *Journal of Geophysical Research*, 116, A06225.  
367 <https://doi.org/10.1029/2011ja016453>.

368 Nishimura, Y., J. Bortnik, W. Li, R. M. Thorne, B. Ni, L. R. Lyons, et al. (2013).  
369 Structures of dayside whistler-mode waves deduced from conjugate diffuse  
370 aurora. *Journal of Geophysical Research: Space Physics*, 118, 664–673.  
371 <https://doi.org/10.1029/2012JA018242>.

372 Omura, Y., and D. Nunn (2011), Triggering process of whistler mode chorus  
373 emissions in the magnetosphere, *J. Geophys. Res.*, 116, A05205,  
374 [doi:10.1029/2010JA016280](https://doi.org/10.1029/2010JA016280).

375 Omura, Y., M. Hikishima, Y. Katoh, D. Summers, and S. Yagitani (2009), Nonlinear  
376 mechanisms of lower-band and upper-band VLF chorus emissions in the  
377 magnetosphere, *J. Geophys. Res.*, 114, A07217, [doi:10.1029/2009JA014206](https://doi.org/10.1029/2009JA014206).

378 Ratcliffe, H., and C. E. J. Watt (2017), Self-consistent formation of a 0.5 cyclotron  
379 frequency gap in magnetospheric whistler mode waves, *J. Geophys. Res. Space*  
380 *Physics*, 122, 8166 – 8180, [doi:10.1002/2017JA024399](https://doi.org/10.1002/2017JA024399).

381 Reeves, G. D., H. E. Spence, M. G. Henderson, S. K. Morley, R. H. W. Friedel, H. O.  
382 Funsten, et al. (2013), Electron acceleration in the heart of the Van Allen  
383 radiation belts. *Science*, 341(6149), 991–994.  
384 <https://doi.org/10.1126/science.1237743>.

385 Ronnmark, K. (1982). WHAMP: Waves in homogeneous, anisotropic,  
386 multicomponent plasmas, Kiruna Geophysical Institute, Report 179. Kiruna,  
387 Sweden.

388 Santolik, O., D. A. Gurnett, J. S. Pickett, M. Parrot, and N. Cornilleau-Wehrin,  
389 Spatio-temporal structure of storm-time chorus (2003), *J. Geophys. Res.*,  
390 108(A7), 1278, doi:10.1029/2002JA009791.

391 Santolik, O., D. A. Gurnett, J. S. Pickett, M. Parrot, and N. Cornilleau-Wehrin  
392 (2005), Central position of the source region of storm-time chorus. *Planetary and*  
393 *Space Science*, 53(1-3), 299–305. <https://doi.org/10.1016/j.pss.2004.09.056>.

394 Santolik, O., et al. (2010), Wave-particle interactions in the equatorial source region  
395 of whistler-mode emissions, *J. Geophys. Res.*, 115, A00F16,  
396 doi:10.1029/2009JA015218.

397 Summers, D., C. Ma, N. P. Meredith, R. B. Horne, R. M. Thorne, D. Heynderickx,  
398 and R. R. Anderson (2002), Model of the energization of outer-zone electrons by  
399 whistler-mode chorus during the October 9, 1990 geomagnetic storm, *Geophys.*  
400 *Res. Lett.*, 29 (24), 2174, doi:10.1029/2002GL016039.

401 Thorne, R. M., B. Ni, X. Tao, R. B. Horne, and N. P. Meredith (2010), Scattering by  
402 chorus waves as the dominant cause of diffuse auroral precipitation. *Nature*,  
403 467(7318), 943–946. <https://doi.org/10.1038/nature09467>.

404 Thorne, R. M., W. Li, B. Ni, Q. Ma, J. Bortnik, L. Chen, et al. (2013), Rapid local  
405 acceleration of relativistic radiation-belt electrons by magnetospheric chorus.  
406 Nature, 504(7480), 411–414. <https://doi.org/10.1038/nature12889>.

407 Tsurutani, B. T. and E. J. Smith (1974), Postmidnight chorus: A substorm  
408 phenomenon. Journal of Geophysical Research, 79(1), 118–127.  
409 <https://doi.org/10.1029/JA079i001p00118>.

410 Wang, S. M., R. S. Wang, S. T. Yao, Q. M. Lu, C. T. Russell, and S. Wang (2019),  
411 Anisotropic electron distributions and whistler waves in a series of the flux  
412 transfer events at the magnetopause. Journal of Geophysical Research: Space  
413 Physics, 124, 1753–1769. <https://doi.org/10.1029/2018JA026417>.

414 Wei, X. H., J. B. Cao, G. C. Zhou, O. Santolik, H. Re `me, I. Dandouras, N.  
415 Cornilleau-Wehrin, E. Lucek, C. M. Carr, and A. Fazakerley (2007), Cluster  
416 observations of waves in the whistler frequency range associated with magnetic  
417 reconnection in the Earth's magnetotail, J. Geophys. Res., 112, A10225,  
418 [doi:10.1029/2006JA011771](https://doi.org/10.1029/2006JA011771).

419 Xiao, F. L., L. J. Chen, H. N. Zheng, and S. Wang (2007), A parametric ray tracing  
420 study of superluminous auroral kilometric radiation wave modes, J. Geophys.  
421 Res., 112, A10214, [doi:10.1029/2006JA012178](https://doi.org/10.1029/2006JA012178).

422 Yue, C., X. An, J. Bortnik, Q. Ma, W. Li, R. M. Thorne, G. D. Reeves, M. Gkioulidou,  
423 D. G. Mitchell, and C. A. Kletzing (2016), The relationship between the

424 macroscopic state of electrons and the properties of chorus waves observed by  
425 the Van Allen Probes, *Geophys. Res. Lett.*, 43, 7804–7812,  
426 doi:10.1002/2016GL070084.

427 **Figure captions:**

428 **Figure 1.** The frequency  $\omega/\Omega_e$  (black lines) and linear growth rate  $\gamma/\Omega_e$  (red lines)  
429 of whistler waves as a function of parallel wave number  $k_{\parallel}v_{th}/\Omega_e$  for two cases with  
430 different relative drift velocities: (a)  $v_d = 0$  and (b)  $v_d = 1.0v_{th}$  in the high-beta  
431 regime. The solid lines indicate parallel propagating whistler waves, whereas dashed  
432 lines correspond to antiparallel propagating whistler waves, hereafter.

433 **Figure 2.** The pitch-angle distribution of electrons for (a) the case shown in Figure 1a  
434 and (b) the case shown in Figure 1b. The coded color denotes the velocity of  
435 electrons.

436 **Figure 3.** The frequency  $\omega_d/\Omega_e$  (black lines) and linear growth rate  $\gamma_d/\Omega_e$  (red  
437 lines) as a function of (a, b) drift velocity  $v_d/v_{th}$ , (c, d) temperature anisotropy  
438  $T_{\perp h}/T_{\parallel h}$ , and (e, f) proportion  $n_h/n_{total}$  of hot electrons.  $\omega_d/\Omega_e$  and  $\gamma_d/\Omega_e$   
439 represent the frequency and growth rate of the most unstable whistler mode in both  
440 parallel (solid lines) and antiparallel (dashed lines) directions, hereafter.

441 **Figure 4.** The frequency  $\omega_m$  (black lines) and linear growth rate  $\gamma_m$  (red lines) as a  
442 function of wave normal angle  $\theta$  for two cases with different relative drift velocities  
443 (a)  $v_d = 0$  and (b)  $v_d = 0.5v_{th}$  in the low-beta regime. Here,  $\omega_m$  and  $\gamma_m$  donate  
444 the frequency and growth rate of the whistler mode with the maximum linear growth  
445 rate at each wave normal angle.

446 **Figure 5.** The pitch-angle distribution of electrons for (a) the case shown in Figure 4a

447 and (b) the case shown in Figure 4b. It has the same format as Figure 2.

448 **Figure 6.** The frequency  $\omega_d/\Omega_e$  (black lines), linear growth rate  $\gamma_d/\Omega_e$  (red lines),  
449 and wave normal angle  $\theta_d$  (blue lines) of whistler mode as a function of (a, b, and c)  
450  $v_d/v_{th}$ , (d, e, and f)  $T_{\perp h}/T_{\parallel h}$ , and (g, h, and i)  $n_h/n_{total}$ . Here,  $\theta_d$  represents the  
451 wave normal angle of the most unstable whistler mode in both directions.

Figure 1.

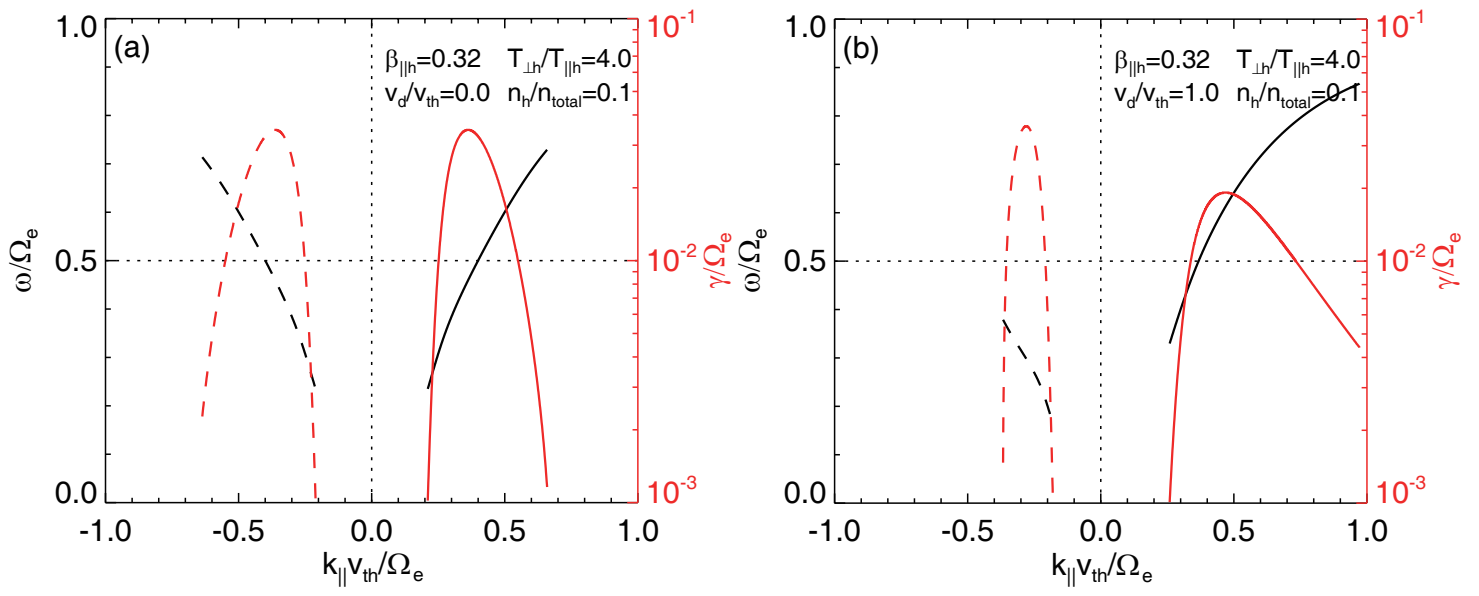


Figure 2.

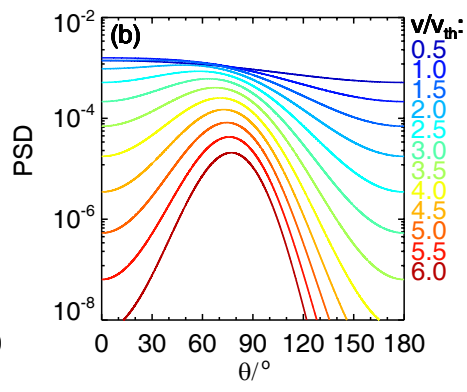
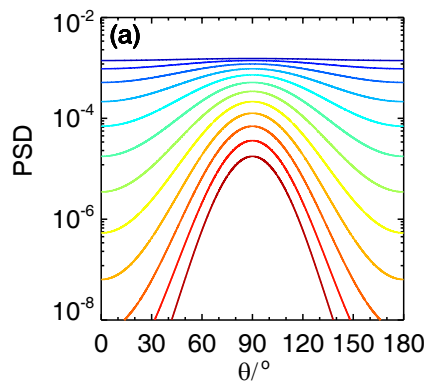
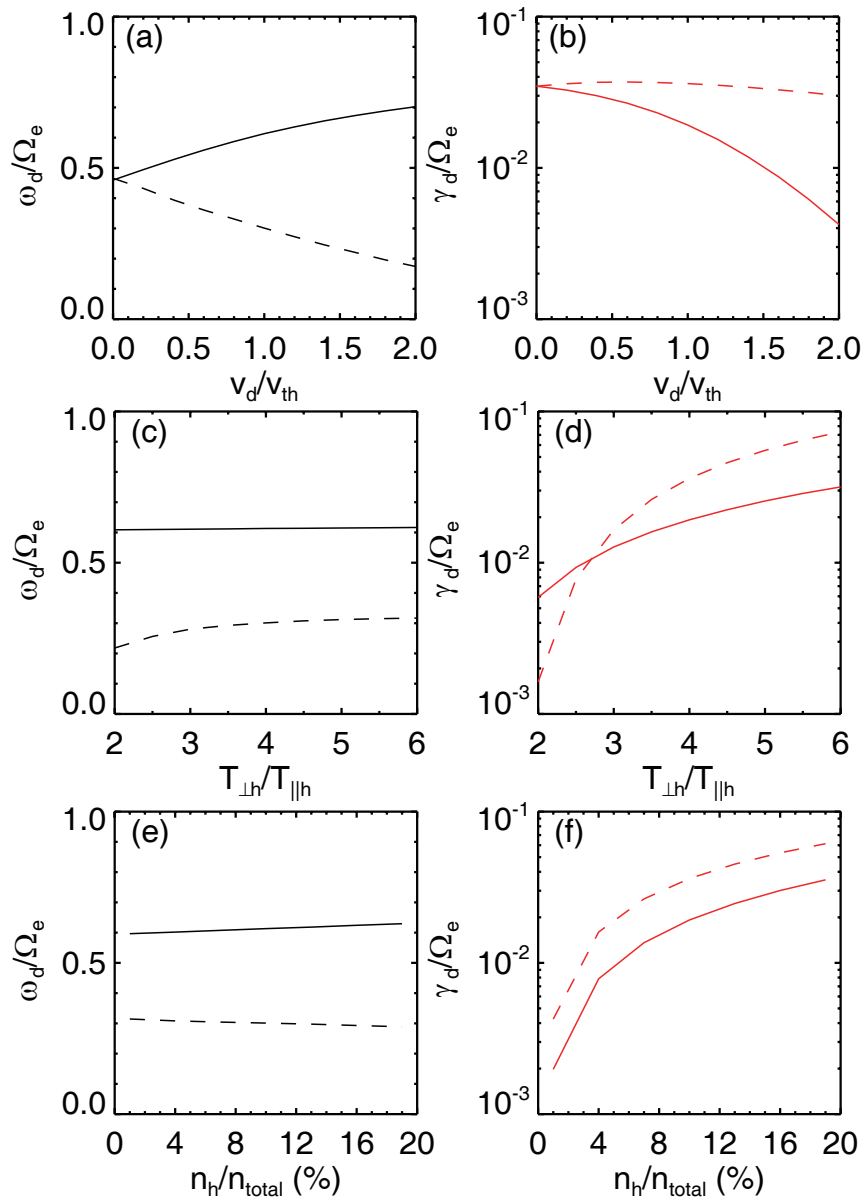


Figure 3.



**Figure 4.**

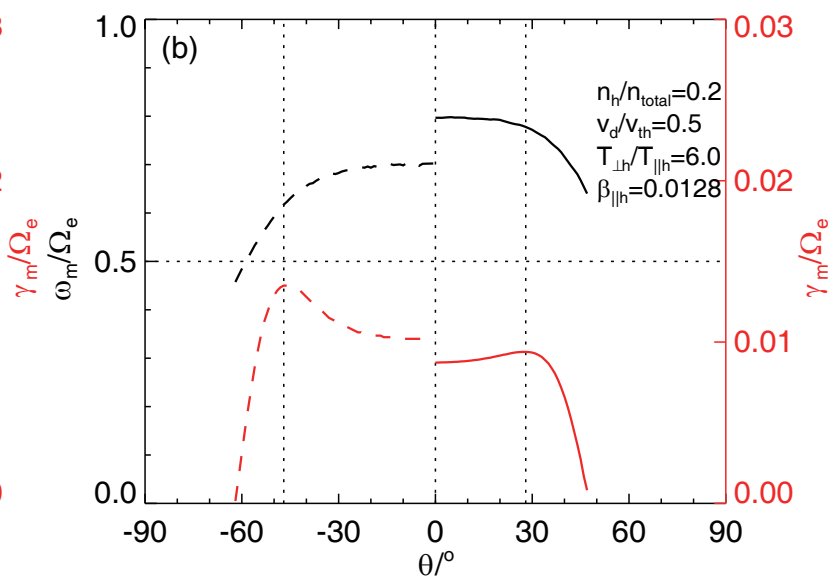
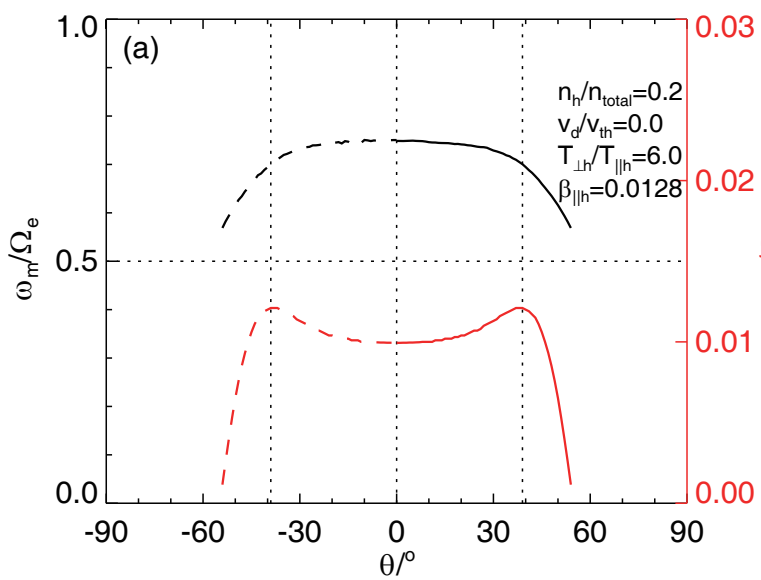


Figure 5.

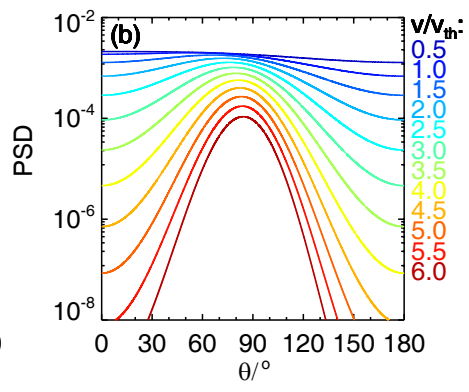
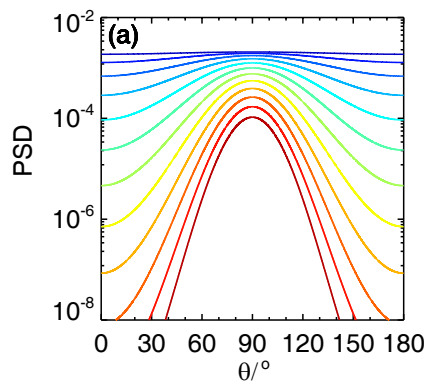


Figure 6.

